Published in final edited form as:
Nano Lett. 2011 September 14; 11(9): 3744–3750. doi:10.1021/nl201782m.

Cancer-Targeted Optical Imaging with Fluorescent Zinc Oxide Nanowires

Hao Hong[1], **Jian Shi**[2], **Yunan Yang**[1], **Yin Zhang**[1], **Jonathan W. Engle**[1], **Robert J. Nickles**[1], **Xudong Wang**[2,*], and **Weibo Cai**[1,3,*]

[1]Departments of Radiology and Medical Physics, University of Wisconsin - Madison, Madison, Wisconsin 53705, USA

[2]Department of Materials Science and Engineering, University of Wisconsin - Madison, Madison 53705, USA

[3]University of Wisconsin Carbone Cancer Center, Madison, Wisconsin 53705, USA

Abstract

Herein we demonstrate that intrinsically fluorescent zinc oxide (ZnO) nanowires (NWs) can be adopted for molecularly targeted imaging of cancer cells, after they are functionalized to render water solubility, biocompatibility, and low cellular toxicity. Optical imaging of integrin $\alpha_v\beta_3$ on U87MG human glioblastoma cells was achieved with RGD peptide-conjugated green fluorescent ZnO NWs, which opened up new avenues of research for investigating ZnO NW-based agents in tumor vasculature-targeted molecular imaging and drug delivery.

Keywords

Zinc oxide (ZnO); nanowire (NW); fluorescence; cancer; molecular imaging; integrin $\alpha_v\beta_3$

Nanotechnology holds tremendous potential for early detection, accurate diagnosis, and personalized treatment of cancer.[1,2] For imaging applications, fluorescence imaging is inexpensive and convenient hence has been widely used in preclinical research, with the best example being quantum dots (QDs).[3–6] Specific targeting of tumor vasculature and tumor cells in vivo has been achieved with various QD-based conjugates.[7–12] However, two major roadblocks for potential widespread application and clinical translation of QDs are their potential toxicity and inefficient delivery. Zinc oxide (ZnO) is well-recognized as a biocompatible multifunctional material with exceptional semiconducting, optical, and piezoelectric properties.[13] It exhibits the most diverse family of nanostructures that can be employed for different applications such as light-emitting diodes, lasers, sensors, actuators, transducers, nanogenerators, etc.[13–18] ZnO is also a wide bandgap semiconductor (3.37 eV) with high exciton binding energy (60 meV), which leads to efficient excitonic blue and near-UV emission.[19]

One of the most important features of ZnO nanomaterials is low toxicity and biodegradability. Zn^{2+} is an indispensable trace element for adults. 9.5 mg and 7.0 mg of Zn^{2+} per day are needed for adult men and women, respectively. Chemically, the surface of ZnO is mostly terminated by -OH groups, which can be readily functionalized by various surface decorating molecules.[20–22] ZnO can slowly dissolve in both acidic (e.g. in tumor cells/microenvironment) and strong basic conditions if the surface is in direct contact with

Corresponding Author: wcai@uwhealth.org OR xudong@engr.wisc.edu.

the solution.[23] These properties make ZnO nanomaterials excellent candidates as biocompatible and biodegradable nanoplatforms for biomedical applications such as DNA delivery,[24,25] magnetic resonance imaging (MRI),[26] and sensing.[27–29] For optical imaging applications, ZnO nanomaterials (e.g. nanorods, nanosheets, nanocrystals) have been employed for sum-frequency generation and fluorescence imaging of cells.[30–34] In addition, ZnO-based QDs have been reported for fluorescence or dual-modality MRI/fluorescence imaging.[25,35–37]

The major obstacles for biomedical applications of ZnO nanomaterials include low-intensity and short-wavelength luminescence of ZnO, limited capability in the size control of ZnO nanostructures (< 200 nm is preferred for in vivo investigations), and sharpness/stiffness of ceramic-based nanostructures (rigid and sharp tips/edges should be avoided to prevent cell/tissue damage). In this study, we synthesized green fluorescent ZnO nanowires (NWs) which overcome these obstacles and demonstrated the proof-of-principle that ZnO NWs can be specifically targeted to cell surface receptors in vitro, which opened up new avenues of future research in tumor-targeted drug delivery. The one-dimensional shape of ZnO NW is highly desirable for efficient tumor targeting since such morphology can readily take advantage of the polyvalency effect.[38]

With future in vivo investigations in mind, we chose integrin $\alpha_v\beta_3$ as the target in this study. Integrin $\alpha_v\beta_3$, which binds to arginine-glycine-aspartic acid (RGD)-containing peptides/proteins,[39,40] is a key protein involved in tumor angiogenesis and metastasis.[41–43] It is over-expressed in a variety of solid tumor types (e.g. melanoma, late stage glioblastoma, breast, prostate, and ovarian cancer),[44] but is not readily detectable in resting endothelial cells or most normal organs, which makes it a universally applicable target for molecular imaging and therapy of cancer. Most importantly, since efficient extravasation is the key hurdle for most nanomaterial-based tumor targeting and imaging, the fact that integrin $\alpha_v\beta_3$ is expressed on both tumor vasculature and tumor cells makes it an ideal target, since extravasation is not required to observe tumor signal.[45,46]

Synthesis and Characterization of ZnO NWs

Vapor deposition of ZnO NWs was conducted in an alumina tube placed inside a single-zone tube furnace. ZnO powder, located at the center of the tube, was used as the precursor. Cooling collars were installed on both ends of the alumina tube to create a temperature gradient for deposition control. The tube was filled with argon at a constant flow rate of 50 cm^3/min and the deposition pressure was kept at 300 mTorr. A polycrystalline alumina substrate was located at 20 cm away from the source, where the local deposition temperature was ~400 °C. The system was heated to 1,000 °C during the first 26 min with a heating rate of 40 °C/min, which was subsequently heated to 1,400 °C with a heating rate of 10 °C/min. After maintaining the system at 1,400 °C for 2 h, the furnace was turned off and the growth system was cooled down to room temperature (RT) naturally under the same argon atmosphere.[47]

Based on scanning electron microscopy (SEM) and transmission electron microscopy (TEM) measurements, the as-synthesized ZnO NWs were of 20–50 nm in diameter and 0.5–1 μm in length, in the form of bundles (Figure 1a). All NWs exhibited a curvy shape without sharp edges (Figure 1b). Such a unique NW morphology is believed to be a result of the competition between oxidation rate and condensation rate of Zn.[47] High condensation rate of Zn under the deposition condition provided a Zn-rich growth environment, which induced continuous nucleation for the formation of bundles of small ZnO NWs. The smooth surfaces were believed to be a result of excess Zn that could diminish the surface energy differences among different crystal facets. More importantly, the as-synthesized ZnO NWs exhibited

exceptionally strong green luminescence (425–575 nm, Figure 1c), likely due to the Zn-rich growth condition which led to a very high oxygen vacancy concentration.[48–50] The green fluorescence is clearly visible when excited with a handheld UV lamp, even after being dispersed in ethanol at a dilute concentration (Figure 1d).

Functionalization of ZnO NWs

Common surface-anchoring molecules for metal oxide (e.g. TiO_2, SnO_2, and ZnO) nanomaterials are carboxylic acids, which can form bidentate coordination bonds with one or two metal atoms.[20–22] Based on previous reports, herein we used 3-mercaptopropionic acid (Sigma-Aldrich) to introduce thiol groups onto the surface of ZnO NWs for further functionalization (Scheme 1). After sonicating the green fluorescent ZnO NWs to form a well-dispersed suspension in ethanol, surface conjugation was carried out. Success of each reaction step was confirmed by monitoring the changes in zeta potential with a Malvern Zeta Sizer Nano (Malvern Instruments). Three milligrams (mg) of 3-mercaptopropionic acid were added to a suspension of 5 mg of ZnO NWs in 2 mL of dichloromethane (DCM). The reaction mixture was stirred at RT for 1 h. After evaporation of DCM, the white solid was collected and washed with ethanol for three times. Two mg of the resulting product (denoted as “NW-SH”) were then reacted with 10 mg of maleimide-polyethylene glycol-succinimidyl carboxy methyl ester (Mal-PEG-SCM; Creative PEGWorks; molecular weight of PEG: 5000) for 1 h at RT in 2 mL of phosphate-buffered saline (PBS, pH = 7.4), in the presence of tris(2-carboxyethyl)phosphine hydrochloride (TCEP; Sigma-Aldrich). The product (denoted as “NW-PEG”) was collected by centrifugation at 8,000 rpm for 5 min and washed repeatedly with ethanol and Millipore-grade water. All ZnO NW conjugates in this work were purified in the same manner.

To synthesize NW-PEG-RGD, ten mg of Mal-PEG-SCM were reacted with 1.3 mg of the c(RGDyK) peptide, where “y” denotes D-tyrosine, in 2 mL of PBS (pH = 8.5) for 4 h at RT. Subsequently, the pH of the reaction mixture was adjusted to 7.0. Two mg of NW-SH was then added and the reaction was allowed to proceed for 1 h at RT in the presence of TCEP. The purified product was denoted as “NW-PEG-RGD”. Both NW-PEG and NW-PEG-RGD were re-suspended in PBS (pH = 7.4) to form a stock solution of 2 mg/mL for further investigation.

The as-synthesized ZnO NW and NW-SH had zeta potential of -29.5 ± 1.8 mV and -21.2 ± 2.4 mV respectively. The zeta potential of NW-PEG and NW-PEG-RGD were -26.1 ± 3.5 mV and -9.1 ± 0.9 mV, respectively. Comparing these values, 3-mercaptopropionic acid and PEG conjugation significant changed the zeta-potential of ZnO NW, and RGD peptide conjugation caused the most pronounced difference. These observations strongly suggested successful surface conjugation of RGD peptides to the NW. To further confirm this aspect, ZnO NWs were mixed with the RGD peptide first and thoroughly washed, which had a zeta potential value of -20.1 ± 4.2 mV, significantly different from that of NW-PEG-RGD (-9.1 ± 0.9 mV). SEM studies of ZnO NWs on the wafer indicated that the morphology and/or size of ZnO NWs did not change after surface functionalization (Figure 1e), which is expected since all reactions were carried out either in organic solvent (i.e. DCM) or neutral aqueous buffer solutions. Furthermore, there was no observable difference between the absorbance/fluorescence spectra of ZnO NW and its conjugates.

Fluorescence Microscopy Studies

To investigate the cancer cell targeting characteristics of functionalized ZnO NWs, taking advantage of their intrinsic fluorescence, U87MG human glioblastoma (high integrin $\alpha_v\beta_3$ expression) and MCF-7 human breast cancer (integrin $\alpha_v\beta_3$-negative) cells were used.[9,11] To identify the optimal concentration and incubation time, a pilot study in live U87MG cells

was performed with different concentrations of NW-PEG-RGD (i.e. 5, 30, and 100 μg/mL), and fluorescence images of the cells were taken at multiple time points after incubation (i.e. 15 min, 30 min, 1 h, and 3 h) using a Nikon Eclipse Ti-E fluorescence microscope (excitation: 330–380 nm; emission: 420 nm long pass; magnification: 200×; exposure: 0.3 s). As can be seen in Figure 2, the fluorescence signal on U87MG cells was substantially weaker at 5 μg/mL of NW-PEG-RGD when compared to that at 30 μg/mL. Increasing the concentration of NW-PEG-RGD to 100 μg/mL did not result in substantial improvement in terms of either the signal intensity or image quality, which may be due to saturation of integrin $\alpha_v\beta_3$ proteins on the cell surface.

Comparing the various time points, incubation for 1 h resulted in the strongest fluorescence intensity on U87MG cells, while 15 and 30 min of incubation appeared to be not sufficient for maximum integrin $\alpha_v\beta_3$ binding of NW-PEG-RGD. Most of the fluorescence signal was at the cell surface since integrin $\alpha_v\beta_3$ is a membrane-bound receptor. The fluorescence signal was substantially lower at 3 h when compared to 1 h post-incubation, likely due to dissolution of ZnO NWs after receptor-mediated endocytosis (endosomes are acidic with a pH around 5 which can dissolve ZnO NWs). Taken together, a concentration of 30 μg/mL and an incubation period of 1 h gave the best imaging results, which was adopted for further studies to confirm the integrin $\alpha_v\beta_3$ specificity of NW-PEG-RGD.

Cell Staining of NW-PEG-RGD is Integrin $\alpha_v\beta_3$-Specific

Cold acetone-fixed U87MG and MCF-7 cells were stained with 30 μg/mL of NW, NW-PEG, NW-PEG-RGD, or NW-PEG-RGD in the presence of 2 μM of c(RGDyK) (i.e. blocking), in a binding buffer (pH 7.4).[9] One hour later, the cells were washed with cold PBS three times and examined under a microscope. For MCF-7 cells which express very low level of integrin $\alpha_v\beta_3$ on the cell surface, little to no fluorescence signal of NW, NW-PEG, or NW-PEG-RGD was observed (Figure 3). For U87MG cells which express high level of integrin $\alpha_v\beta_3$, intense fluorescence signal was observed for NW-PEG-RGD but not for NW or NW-PEG. Blocking with the c(RGDyK) peptide resulted in substantially lower fluorescence signal in U87MG cells, which confirmed the high affinity and integrin $\alpha_v\beta_3$-specific binding of NW-PEG-RGD. Taken together, these cell-based studies demonstrated that NW-PEG-RGD can specifically recognize integrin $\alpha_v\beta_3$ on cell surface with minimal non-specific binding. In addition, there is minimal non-specific binding of NW and NW-PEG to U87MG and MCF-7 cells.

Such promising in vitro findings warrant further investigation of ZnO NWs for in vivo applications, where they may serve as a nanoplatform for image-guided tumor vasculature-targeted drug delivery. For optical imaging in vivo, fluorescence emission in the near-infrared (NIR; 700–900 nm) region is preferred.[6] Doping with Ce[51] or Eu[52] may be investigated in the future to achieve red-to-NIR luminescence of ZnO NWs. Optical imaging, which takes advantage of its intrinsic fluorescence, can provide convenient tracking of ZnO NW conjugates in small animal models. Furthermore, the intrinsic fluorescence of ZnO NWs can enable microscopy/histology studies without an exogenous dye, which can serve as a convenient and robust means for validating in vivo results.

An alternative and complementary approach to study ZnO NW distribution in vivo is via radionuclide-based imaging techniques, such as positron emission tomography (PET).[53,54] Attaching PET isotopes to ZnO NW conjugates is highly beneficial since PET is very sensitive (down to 10^{-12} molar), quantitative, and clinically relevant with superb tissue penetration.[55] One scenario where such a dual-modality PET/optical agent is particularly useful is that an initial whole-body PET scan can be carried out to identify the location of tumor(s), and optical imaging can be subsequently used to guide tumor resection.

PET Imaging with ^{64}Cu-Labeled ZnO NWs

As a proof-of-principle pilot study, we labeled ZnO NWs with ^{64}Cu ($t_{1/2}$: 12.7 h) and evaluated the biodistribution with PET in three six-week-old female Balb/c mice. The macrocyclic chelator DOTA (1, 4, 7, 10-tetraazacyclododecane-1, 4, 7, 10-tetraacetic acid) has been widely used for ^{64}Cu-labeling and PET imaging.[56–58] To synthesize NW-PEG-DOTA, ten mg of Mal-PEG-NH_2 (molecular weight of PEG: 5000) were mixed with 1.5 mg of DOTA-*N*-hydroxysuccinimide (NHS) ester in 2 mL of PBS (pH ~ 8.5) for 4 h at RT. Subsequently, the pH of the reaction mixture was adjusted to 7.0. Two mg of NW-SH were added and the reaction was allowed to proceed for 1 h at RT in the presence of TCEP. The product, NW-PEG-DOTA, was purified and re-suspended in PBS.

For ^{64}Cu-labeling, 111 MBq of $^{64}CuCl_2$ was diluted in 300 μL of 0.1 M sodium acetate buffer (pH ~6.5) and added to 200 μg of NW-PEG-DOTA. The reaction mixture was incubated for 30 min at 40 °C with constant shaking. NW-PEG-DOTA-^{64}Cu was then purified and re-constituted in PBS. The decay-corrected radiolabeling yield was ~85%. Mice were each injected intravenously with 5–10 MBq of NW-PEG-DOTA-^{64}Cu and scanned in a microPET/microCT Inveon rodent model scanner (Siemens Medical Solutions USA, Inc.). All animal studies were conducted under a protocol approved by the University of Wisconsin Institutional Animal Care and Use Committee. Ten-min static PET scans, reconstructed using a two-dimensional filtered back-projection algorithm with no attenuation/scatter correction,[59] were performed at 20 min and 20 h post-injection to non-invasive examine the biodistribution of NW-PEG-DOTA-^{64}Cu. Similar to most nanomaterials, non-targeted ZnO NWs primarily accumulated in the liver (Figure 4), the major organ of the reticuloendothelial system (RES).[60–63]

Cytotoxicity of ZnO NW Conjugates

Cytotoxicity of ZnO NW and its conjugates were examined in both U87MG and MCF-7 cells using the 3-(4,5-dimethylthiazol-2-yl)-2,5-diphenyltetrazolium bromide (MTT) assay, similar as described previously.[63,64] Cells were seeded at a density of 1.5×10^4 cells/well in 96-well plates, allowed to grow for 48 h, and exposed to various concentrations of NW, NW-PEG, or NW-PEG-RGD for 24 h. The absorbance of each well at 570 nm (A_{570}) was measured with a Spectramax Plus384 absorbance microplate reader (Molecular Devices), using the absorbance at 630 nm (A_{630}) as a reference. $A_{570} - A_{630}$ was taken as the index of cell viability, with the $A_{570} - A_{630}$ of control untreated cells set as 100% viable. The percentage of viability was calculated using the formula $[(A_{570} - A_{630})_{sample}/(A_{570} - A_{630})_{control}] \times 100$.

At a concentration of 30 μg/mL, the toxicity of NW-PEG-RGD and NW-PEG was low and amenable for cellular imaging (Figure 5). Overall, PEG conjugation reduced the toxicity of ZnO NW in both U87MG and MCF-7 cells. The toxicity of NW-PEG-RGD was higher than that of NW and NW-PEG in U87MG cells at concentrations > 20 μg/mL. Since U87MG cells express high level of integrin $\alpha_v\beta_3$, which is critical for cell adhesion to the wells, high concentration of RGD peptides on ZnO NWs likely contributed to its cellular toxicity. In addition, NW-PEG-RGD can be internalized into U87MG cells (through receptor-mediated endocytosis) more readily than NW/NW-PEG and dissolve in the endosome and/or lysosome. The high intracellular concentration of Zn^{2+} may also have caused the enhanced toxicity of NW-PEG-RGD in U87MG cells. On the other hand, the toxicity of NW-PEG-RGD was lower than that of NW and similar to that of NW-PEG in MCF-7 cells. Since MCF-7 cells do not express significant level of integrin $\alpha_v\beta_3$, high concentration of RGD peptides on ZnO NWs did not have significant impact on the cellular toxicity.

Many studies have focused on the biocompatibility of ZnO nanomaterials without surface modification. Although some reports showed that ZnO nanomaterials were toxic above certain concentrations,[65–67] which could be attributed to the dissolved Zn^{2+} in the culture medium or inside cells, others have demonstrated that ZnO nanomaterials were non-toxic,[68] selectively toxic to bacteria or cancer cells,[33,69] or useful as adhesion-resistant biomaterials.[70] It has been shown that the safety of ZnO nanoparticles could be improved by decreasing ZnO dissolution through Fe doping or surface capping.[71,72] For biomedical applications of nanomaterials, surface modification is crucial. The versatile chemistry of ZnO nanomaterials can enable facile conjugation of various biocompatible polymers, imaging labels, drugs, among others. The key question is not how toxic “naked” ZnO nanomaterials are, but how to functionalize them so that they do not exhibit significant toxicity thereby can be used in biological systems.

In conclusion, herein we demonstrated for the first time that intrinsically fluorescent ZnO NWs can be employed for cancer-targeted optical imaging, upon surface functionalization to render water solubility, biocompatibility, and low cellular toxicity. Much can be done in the future to further improve the (fluorescence) properties of ZnO NWs for in vivo targeting/imaging of tumor vasculature. For example, further reducing the size of ZnO NWs may improve the tumor targeting efficacy; Fine-tuning the in vitro/in vivo stability of ZnO NW conjugates will make them circulate long enough to allow efficient tumor vasculature targeting, and subsequently dissolve over time to release the therapeutic load once they reach the tumor tissue. With many desirable properties such as biocompatibility, versatile chemistry, and intrinsic fluorescence, ZnO NWs can serve as a novel nanoplatform for cancer imaging and therapy.

Acknowledgments

This work is supported, in part, by the University of Wisconsin Carbone Cancer Center, University of Wisconsin Graduate School, a DOD BCRP Postdoctoral Fellowship, a DOD PCRP IDEA Award, NCRR 1UL1RR025011, the National Science Foundation under Grant No. DMR-0905914, and the NIH through the UW Radiological Sciences Training Program 5 T32 CA009206-32.

REFERENCES

1. Whitesides GM. Small. 2005; 1:172–179. [PubMed: 17193427]
2. Ferrari M. Nat. Rev. Cancer. 2005; 5:161–171. [PubMed: 15738981]
3. Alivisatos AP, Gu W, Larabell C. Annu. Rev. Biomed. Eng. 2005; 7:55–76. [PubMed: 16004566]
4. Michalet X, Pinaud FF, Bentolila LA, Tsay JM, Doose S, Li JJ, Sundaresan G, Wu AM, Gambhir SS, Weiss S. Science. 2005; 307:538–544. [PubMed: 15681376]
5. Medintz IL, Uyeda HT, Goldman ER, Mattoussi H. Nat. Mater. 2005; 4:435–446. [PubMed: 15928695]
6. Cai W, Hsu AR, Li ZB, Chen X. Nanoscale Res. Lett. 2007; 2:265–281. [PubMed: 21394238]
7. Akerman ME, Chan WCW, Laakkonen P, Bhatia SN, Ruoslahti E. Proc. Natl. Acad. Sci. USA. 2002; 99:12617–12621. [PubMed: 12235356]
8. Gao X, Cui Y, Levenson RM, Chung LWK, Nie S. Nat. Biotechnol. 2004; 22:969–976. [PubMed: 15258594]
9. Cai W, Shin DW, Chen K, Gheysens O, Cao Q, Wang SX, Gambhir SS, Chen X. Nano Lett. 2006; 6:669–676. [PubMed: 16608262]
10. Tada H, Higuchi H, Wanatabe TM, Ohuchi N. Cancer Res. 2007; 67:1138–1144. [PubMed: 17283148]
11. Cai W, Chen K, Li ZB, Gambhir SS, Chen X. J. Nucl. Med. 2007; 48:1862–1870. [PubMed: 17942800]
12. Chen K, Li ZB, Wang H, Cai W, Chen X. Eur. J. Nucl. Med. Mol. Imaging. 2008; 35:2235–2244. [PubMed: 18566815]

13. Wang ZL. ACS Nano. 2008; 2:1987–1992. [PubMed: 19206442]
14. Fan Z, Lu JG. J. Nanosci. Nanotechnol. 2005; 5:1561–1573. [PubMed: 16245516]
15. Huang MH, Wu Y, Feick H, Tran N, Weber E, Yang P. Adv. Mater. 2001; 13:113–116.
16. Wang X, Liu J, Song J, Wang ZL. Nano Lett. 2007; 7:2475–2479. [PubMed: 17604406]
17. Lao CS, Park M-C, Kuang Q, Deng Y, Sood AK, Polla DL, Wang ZL. J. Am. Chem. Soc. 2007; 129:12096–12097. [PubMed: 17880088]
18. Wang X, Song J, Summers CJ, Ryou JH, Li P, Dupuis RD, Wang ZL. J. Phys. Chem. B. 2006; 110:7720–7724. [PubMed: 16610866]
19. Özgür Ü, Alivov YI, Liu C, Teke A, Reshchikov MA, Doğan S, Avrutin V, Cho S-J, Morkoç H. J. Appl. Phys. 2005; 98 041301.
20. Galoppini E. Coord. Chem. Rev. 2004; 248:1283–1297.
21. Liu D, Wu W, Qiu Y, Yang S, Xiao S, Wang QQ, Ding L, Wang J. Langmuir. 2008; 24:5052–5059. [PubMed: 18370437]
22. Taratula O, Galoppini E, Wang D, Chu D, Zhang Z, Chen H, Saraf G, Lu Y. J. Phys. Chem. B. 2006; 110:6506–6515. [PubMed: 16570948]
23. Zhou J, Xu NS, Wang ZL. Adv. Mater. 2006; 18:2432–2435.
24. Nie L, Gao L, Feng P, Zhang J, Fu X, Liu Y, Yan X, Wang T. Small. 2006; 2:621–625. [PubMed: 17193097]
25. Zhang P, Liu W. Biomaterials. 2010; 31:3087–3094. [PubMed: 20096454]
26. Barcena C, Sra AK, Chaubey GS, Khemtong C, Liu JP, Gao J. Chem. Commun. 2008:2224–2226.
27. Chang CC, Chiu NF, Lin DS, Chu-Su Y, Liang YH, Lin CW. Anal. Chem. 82:1207–1212. [PubMed: 20102177]
28. Al-Hilli SM, Willander M, Ost A, Stralfors P. J. Appl. Phys. 2007; 102:084304–084305.
29. Dorfman A, Kumar N, Hahm JI. Langmuir. 2006; 22:4890–4895. [PubMed: 16700567]
30. Kachynski AV, Kuzmin AN, Nyk M, Roy I, Prasad PN. J. Phys. Chem. C Nanomater. Interfaces. 2008; 112:10721–10724. [PubMed: 19633706]
31. Xiong HM, Xu Y, Ren QG, Xia YY. J. Am. Chem. Soc. 2008; 130:7522–7523. [PubMed: 18498161]
32. Guell F, Osso JO, Goni AR, Cornet A, Morante JR. Nanotechnology. 2009; 20 315701.
33. Wang H, Wingett D, Engelhard MH, Feris K, Reddy KM, Turner P, Layne J, Hanley C, Bell J, Tenne D, Wang C, Punnoose A. J. Mater. Sci. Mater. Med. 2009; 20:11–22. [PubMed: 18651111]
34. Wang H, Jiang H, Zhang H, Zhou Y, Wu C, Zhao J, Ba L, Wang X. J. Nanosci. Nanotechnol. 2011; 11:1117–1122. [PubMed: 21456148]
35. Liu Y, Ai K, Yuan Q, Lu L. Biomaterials. 2011; 32:1185–1192. [PubMed: 21055806]
36. Sudhagar S, Sathya S, Pandian K, Lakshmi BS. Biotechnol. Lett. 2011 Epub.
37. Singh SP. J. Biomed. Nanotechnol. 2011; 7:95–97. [PubMed: 21485821]
38. Mammen M, Chio S, Whitesides GM. Angew. Chem. Int. Ed. Engl. 1998; 37:2755–2794.
39. Xiong JP, Stehle T, Zhang R, Joachimiak A, Frech M, Goodman SL, Arnaout MA, Diefenbach B, Dunker R, Scott DL. Science. 2002; 296:151–155. [PubMed: 11884718]
40. Cai W, Niu G, Chen X. Curr. Pharm. Des. 2008; 14:2943–2973. [PubMed: 18991712]
41. Hood JD, Cheresh DA. Nat. Rev. Cancer. 2002; 2:91–100. [PubMed: 12635172]
42. Bergers G, Benjamin LE. Nat. Rev. Cancer. 2003; 3:401–410. [PubMed: 12778130]
43. Cai W, Chen X. J. Nucl. Med. 2008; 49 Suppl 2:113S–128S. [PubMed: 18523069]
44. Cai W, Chen X. Anti-Cancer Agents Med. Chem. 2006; 6:407–428.
45. Hong H, Zhang Y, Sun J, Cai W. Nano Today. 2009; 4:399–413. [PubMed: 20161038]
46. Ruoslahti E, Bhatia SN, Sailor MJ. J. Cell. Biol. 2010; 188:759–768. [PubMed: 20231381]
47. Shi J, Hong H, Ding Y, Yang Y, Wang F, Cai W, Wang X. J. Mater. Chem. 2011; 21:9000–9008. [PubMed: 21743779]
48. Heo YW, Norton DP, Pearton SJ. J. Appl. Phys. 2005; 98:073502–073506.
49. Leiter F, Alves H, Pfisterer D, Romanov NG, Hofmann DM, Meyer BK. Physica B. 2003; 340–342:201–204.

50. Vanheusden K, Seager CH, Warren WL, Tallant DR, Voigt J. A. Appl. Phys. Lett. 1996; 68:403–405.
51. Sofiani Z, Derkowska B, Dalasinski P, Wojdyla M, Dabos-Seignon S, Lamrani MA, Dghoughi L, Bala W, Addou M, Sahraoui B. Opt. Commun. 2006; 267:433–439.
52. Lima SAM, Davolos MR, Quirino WG, Legnani C, Cremona M. Appl. Phys. Lett. 2007; 90:023503–023503.
53. Cai W, Chen X. Small. 2007; 3:1840–1854. [PubMed: 17943716]
54. Hong H, Gao T, Cai W. Nano Today. 2009; 4:252–261. [PubMed: 21754949]
55. Gambhir SS. Nat. Rev. Cancer. 2002; 2:683–693. [PubMed: 12209157]
56. Wadas TJ, Wong EH, Weisman GR, Anderson CJ. Curr. Pharm. Des. 2007; 13:3–16. [PubMed: 17266585]
57. Cai W, Chen K, Mohamedali KA, Cao Q, Gambhir SS, Rosenblum MG, Chen X. J. Nucl. Med. 2006; 47:2048–2056. [PubMed: 17138749]
58. Cai W, Wu Y, Chen K, Cao Q, Tice DA, Chen X. Cancer Res. 2006; 66:9673–9681. [PubMed: 17018625]
59. Hong H, Yang Y, Zhang Y, Engle JW, Barnhart TE, Nickles RJ, Leigh BR, Cai W. Eur. J. Nucl. Med. Mol. Imaging. 2011; 38:1335–1343. [PubMed: 21373764]
60. Soo Choi H, Liu W, Misra P, Tanaka E, Zimmer JP, Itty Ipe B, Bawendi MG, Frangioni JV. Nat. Biotechnol. 2007; 25:1165–1170. [PubMed: 17891134]
61. Liu Z, Cai W, He L, Nakayama N, Chen K, Sun X, Chen X, Dai H. Nat. Nanotechnol. 2007; 2:47–52. [PubMed: 18654207]
62. Schipper ML, Iyer G, Koh AL, Cheng Z, Ebenstein Y, Aharoni A, Keren S, Bentolila LA, Li J, Rao J, Chen X, Banin U, Wu AM, Sinclair R, Weiss S, Gambhir SS. Small. 2009; 5:126–134. [PubMed: 19051182]
63. Yang X, Hong H, Grailer JJ, Rowland IJ, Javadi A, Hurley SA, Xiao Y, Yang Y, Zhang Y, Nickles RJ, Cai W, Steeber DA, Gong S. Biomaterials. 2011; 32:4151–4160. [PubMed: 21367450]
64. Niu G, Cai W, Chen K, Chen X. Mol. Imaging Biol. 2008; 10:99–106. [PubMed: 18157579]
65. Xia T, Kovochich M, Liong M, Madler L, Gilbert B, Shi H, Yeh JI, Zink JI, Nel AE. ACS Nano. 2008; 2:2121–2134. [PubMed: 19206459]
66. Deng X, Luan Q, Chen W, Wang Y, Wu M, Zhang H, Jiao Z. Nanotechnology. 2009; 20 115101.
67. Muller KH, Kulkarni J, Motskin M, Goode A, Winship P, Skepper JN, Ryan MP, Porter AE. ACS Nano. 2010; 4:6767–6779. [PubMed: 20949917]
68. Li Z, Yang R, Yu M, Bai F, Li C, Wang ZL. J. Phys. Chem. C. 2008; 112:20114–20117.
69. Banoee M, Seif S, Nazari ZE, Jafari-Fesharaki P, Shahverdi HR, Moballegh A, Moghaddam KM, Shahverdi AR. J. Biomed. Mater. Res. B Appl. Biomater. 2010; 93:557–561. [PubMed: 20225250]
70. Lee J, Kang BS, Hicks B, Chancellor TF Jr, Chu BH, Wang HT, Keselowsky BG, Ren F, Lele TP. Biomaterials. 2008; 29:3743–3749. [PubMed: 18550161]
71. George S, Pokhrel S, Xia T, Gilbert B, Ji Z, Schowalter M, Rosenauer A, Damoiseaux R, Bradley KA, Madler L, Nel AE. ACS Nano. 4:15–29. [PubMed: 20043640]
72. Nair S, Sasidharan A, Divya Rani VV, Menon D, Manzoor K, Raina S. J. Mater. Sci. Mater. Med. 2009; 20 Suppl 1:S235–S241. [PubMed: 18716714]

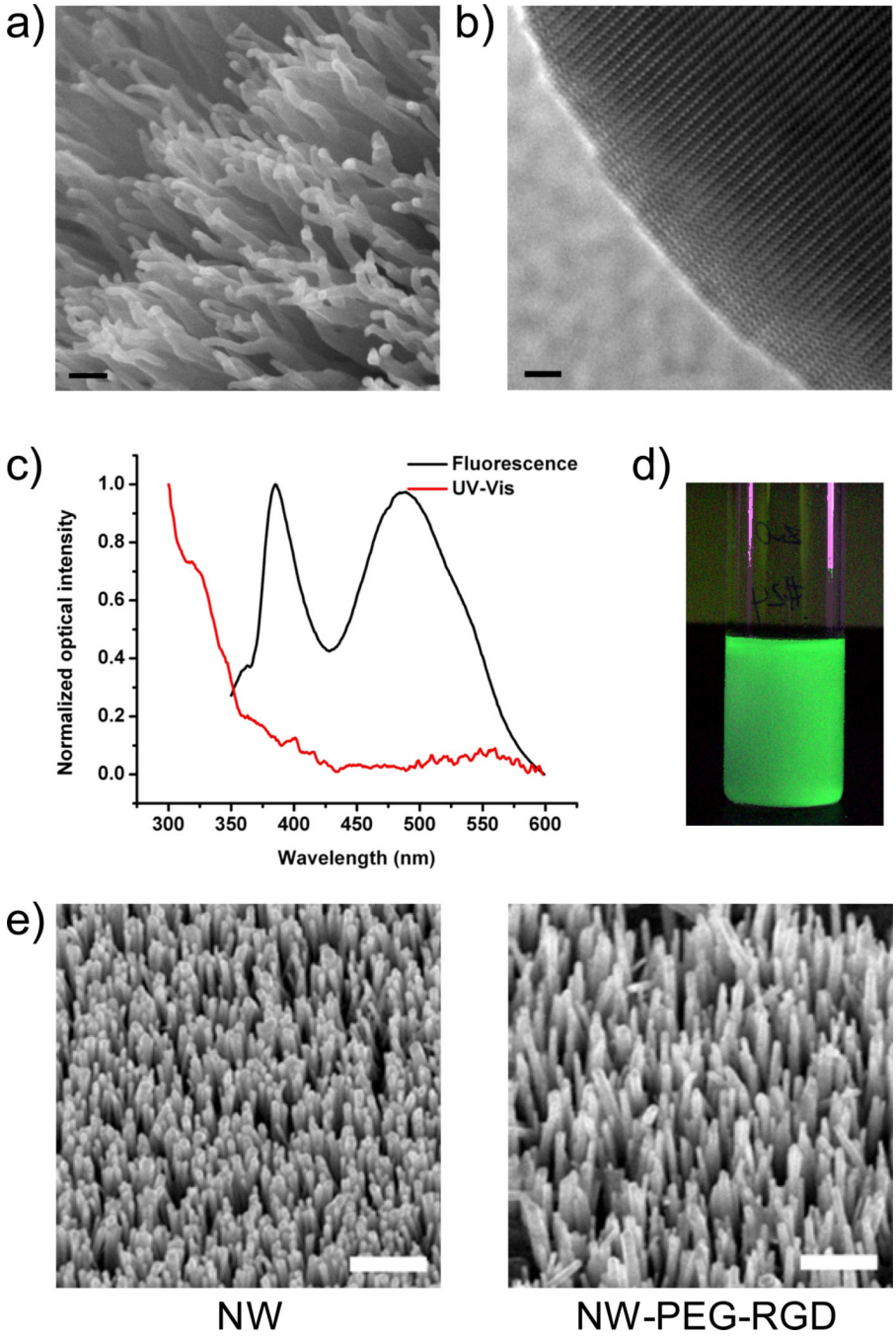

Figure 1.

Characterization of ZnO NWs. (a) A SEM image of ZnO NW bundles. Scale bar: 100 nm. (b) A TEM image of the tip of a ZnO NW. Scale bar: 2 nm. (c) UV-Vis absorbance and fluorescence spectra of ZnO NW in solution. (d) A photograph of ZnO NW solution in ethanol under UV excitation. (e) SEM images of ZnO NWs before and after surface functionalization revealed no significant change in size or morphology. Scale bar: 1 μm. Some ZnO NWs detached from the wafer after 3 steps of reaction. Thus, the density of NW-PEG-RGD is lower than the as-synthesized ZnO NW.

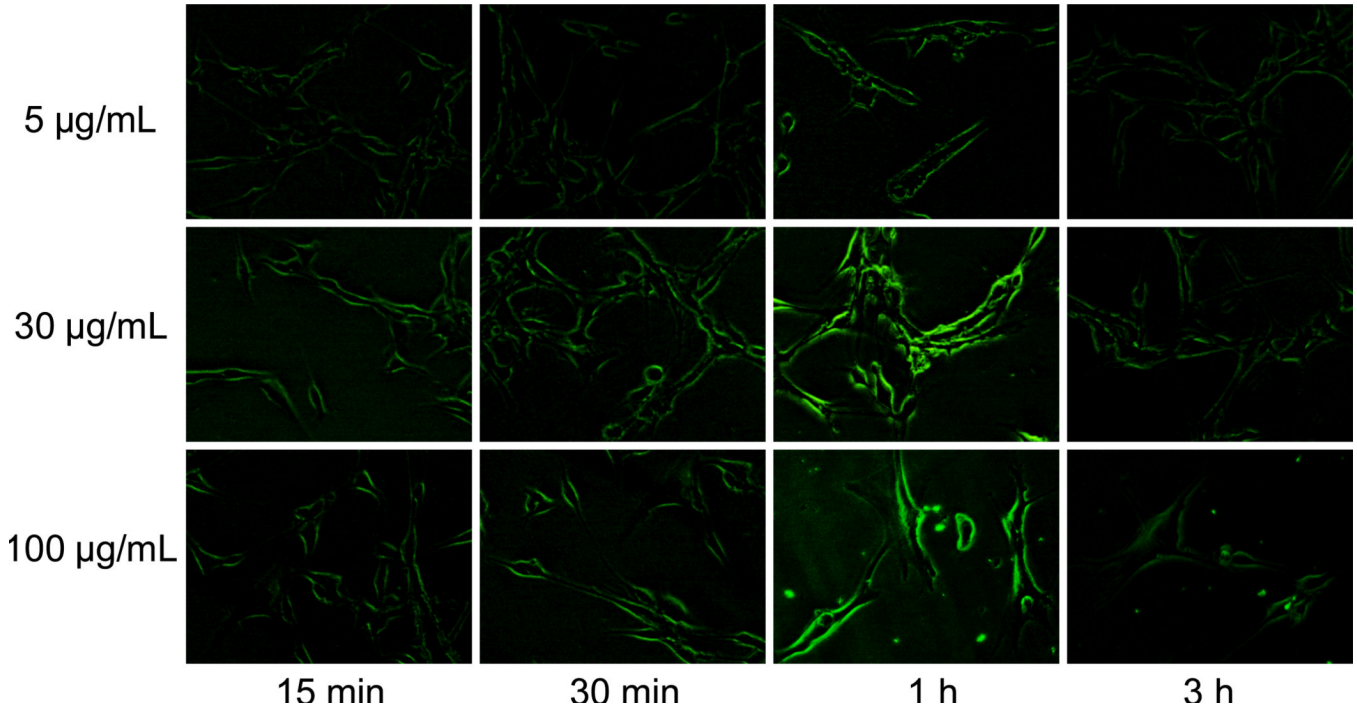

Figure 2.
Serial fluorescence imaging of integrin $\alpha_v\beta_3$ on live U87MG human glioblastoma cells with various concentrations of NW-PEG-RGD. All fluorescence images were acquired under the same condition and displayed using the same scale. Magnification: 200×.

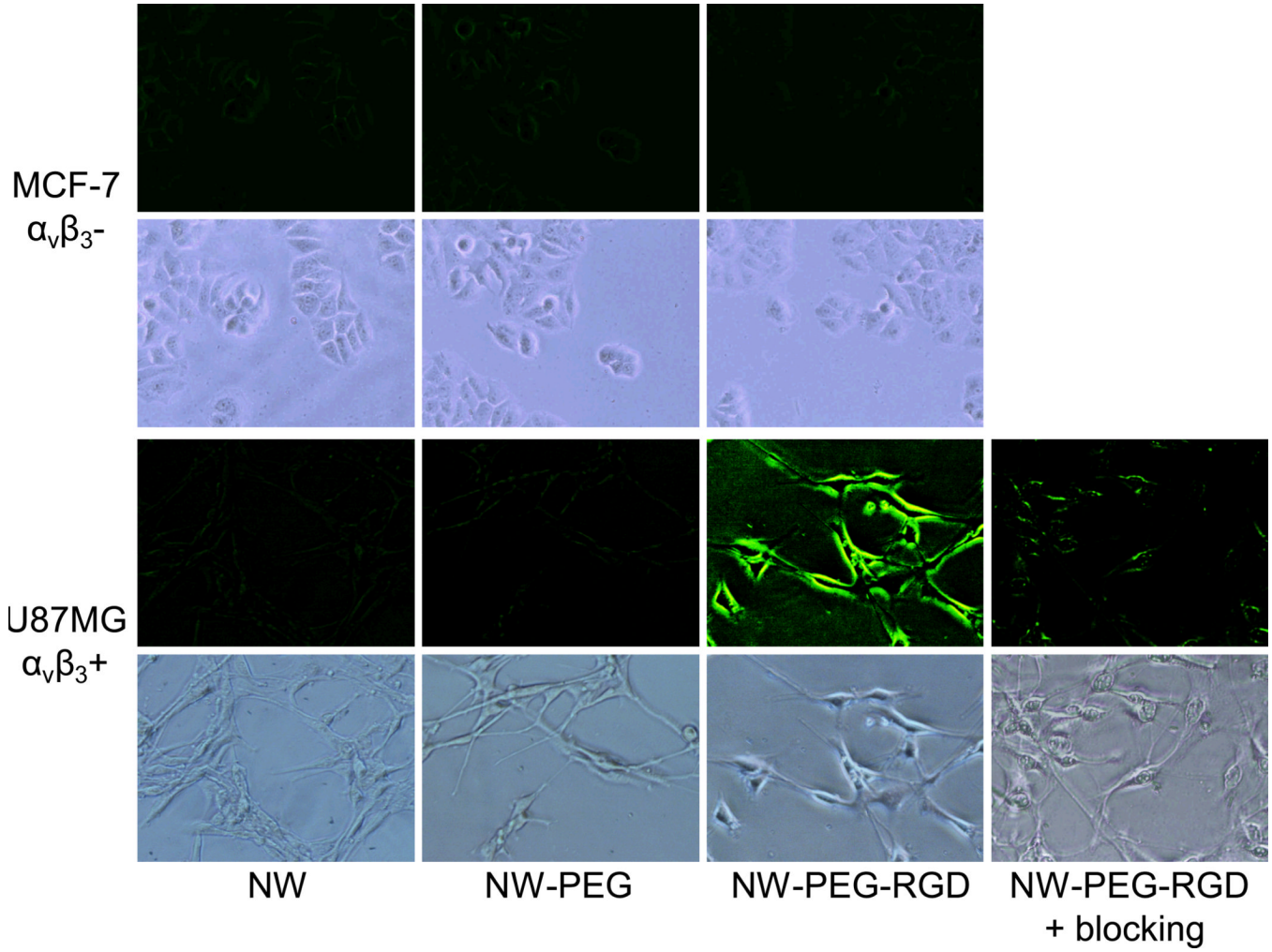

Figure 3.
Fluorescence imaging of integrin $\alpha_v\beta_3$ expression on fixed U87MG human glioblastma and MCF-7 human breast cancer cells with ZnO NW and its conjugates. A concentration of 30 μg/mL (based on ZnO NW) and an incubation period of 1 h was adopted. “Blocking” denotes co-incubation with 2 μM of c(RGDyK) peptide. All fluorescence images were acquired under the same condition and displayed using the same scale. Magnification: 200×.

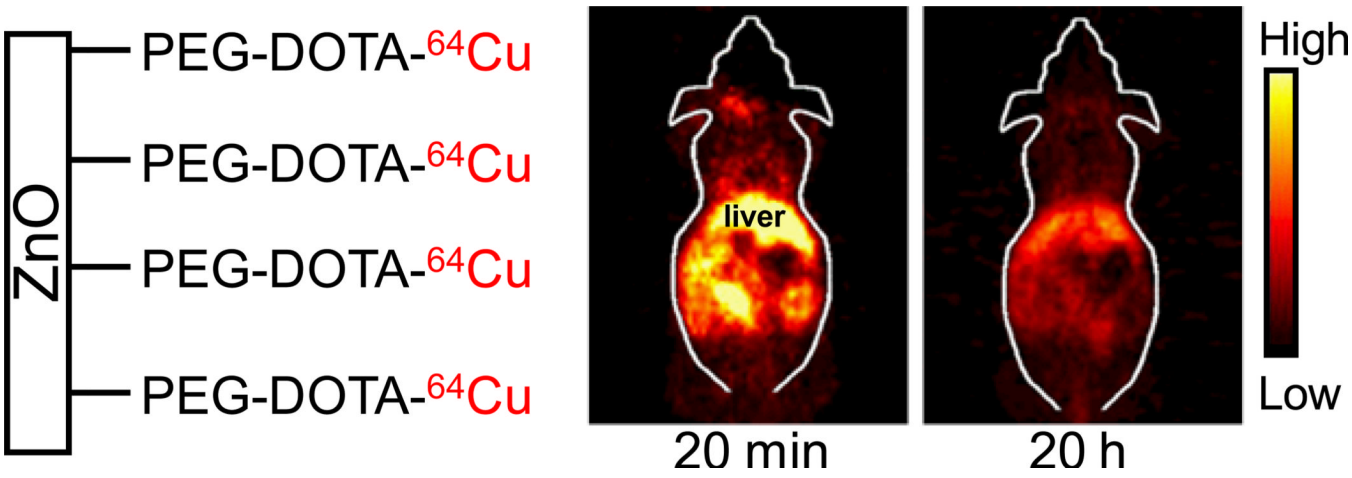

Figure 4.
Representatives PET images of NW-PEG-DOTA-^{64}Cu at 20 min and 20 h post-injection into female Balb/c mice.

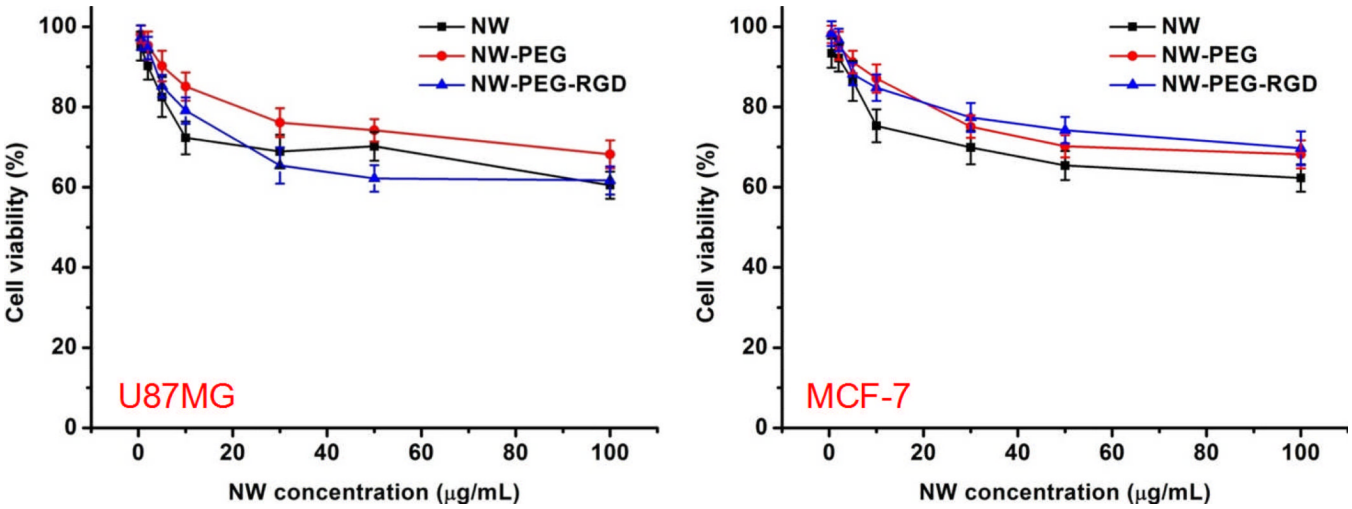

Figure 5.
Cytotoxicity of ZnO NW and its conjugates at various concentrations.

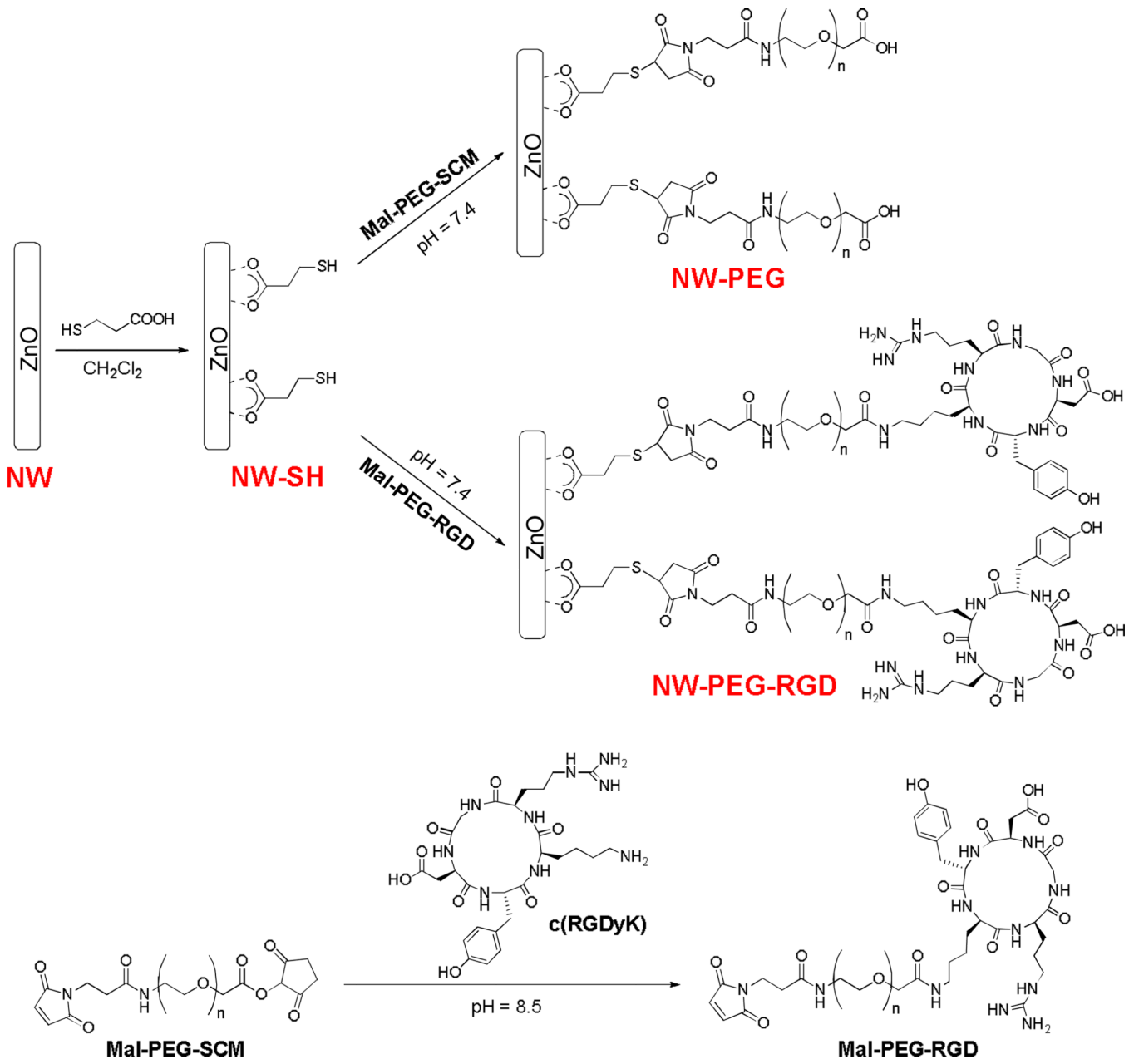

Scheme 1.
The syntheses of ZnO NW conjugates.